Korean J. Chem. Eng., 35(2), 548-556 (2018)
DOI: 10.1007/s11814-017-0281-0

pISSN: 0256-1115
eISSN: 1975-7220

Enhancement in photocatalytic degradation of methylene blue by $LaFeO_3$-GO integrated photocatalyst-adsorbents under visible light irradiation

Muhazri Abd Mutalib*, Farhana Aziz,***,†, Nur Aisyah Jamaludin**,***, Norsyazwani Yahya**,***, Ahmad Fauzi Ismail**,***, Mohamad Azuwa Mohamed****, Mohd Zamri Mohd Yusop**,*****, Wan Norharyati Wan Salleh**,***, Juhana Jaafar**,***, and Norhaniza Yusof**,***

*Solar Energy Research Institute (SERI), Universiti Kebangsaan Malaysia (UKM), 43600 Bangi, Selangor, Malaysia
**Advanced Membrane Technology Research Centre (AMTEC), Universiti Teknologi Malaysia, 81310, UTM Johor Bahru, Johor, Malaysia
***Faculty of Chemical and Energy Engineering, Universiti Teknologi Malaysia, 81310, UTM Johor Bahru, Johor, Malaysia
****Fuel Cell Institute (SELFUEL), Universiti Kebangsaan Malaysia, 43600 UKM Bangi, Selangor, Malaysia
*****Faculty of Mechanical Engineering, Universiti Teknologi Malaysia, 81310, UTM Johor Bahru, Johor, Malaysia
(*Received 13 June 2017 • accepted 7 October 2017*)

Abstract−Perovskite $LaFeO_3$ photocatalyst prepared by using sol-gel glucose method was assembled on graphene oxide sheets to produce integrated photocatalyst-adsorbents (IPCA) and investigated as photocatalyst for the degradation of methylene blue under visible light irradiation. The prepared photocatalyst was characterized by FTIR, XRD, FESEM, BET specific surface area measurement, TEM/HRTEM and UV-Vis spectroscopy analysis. The FTIR, FESEM and TEM analysis has suggested that the photocatalyst $LaFeO_3$ has been successfully embedded at the surface of the graphene oxide (GO) sheets due to a strong interaction between the photocatalyst and the adsorbents matrix. Methylene blue degradation shows that IPCA possesses higher photodegradation kinetics compared to bare $LaFeO_3$ photocatalyst. The resultant photocatalyst also possesses magnetic properties which can overcome the difficulty in recollecting and removal of photocatalyst suspension in water after photocatalytic treatment.

Keywords: Integrated Photocatalyst-adsorbents (IPCA), Perovskite $LaFeO_3$ Photocatalyst, Photodegradation, Magnetic, Graphene Oxide

INTRODUCTION

The utilization of composite material at the nanoscale level by supporting nanomaterials onto porous network has been featured in numerous applications with notable performance enhancement [1-4]. The porous network provides increased surface contact for the nanoparticles to combat agglomeration of nanoparticles, which can cause severe performance reduction [5]. The synthesis of nanocomposites with catalytic nanoparticles supported on porous medium has gained considerable attention for advanced oxidation processes (AOPs), photocatalysis application, which could be a very promising aspect for future technologies in wastewater treatment application [6-8]. AOPs are generally defined as water treatment technologies generating hydroxyl radicals which are responsible for organic degradation. Due to their strong unselective oxidative power, they are able to oxidize and mineralize almost any organic molecule, yielding CO_2 and inorganic ions as final products. The generation of hydroxyl radicals can be initiated by primary oxidants (hydrogen peroxide, ozone) energy sources (UV light, ultrasonic and heat) or catalysts (titania, zinc oxide and Fenton reagent) [9-11]. Among AOPs, photocatalysis is an interesting alternative process that can remove the emerging contaminants at ambient temperature and pressure by oxidation. Additionally, perovskite-based catalyst has been receiving increased attention due to their photocatalytic properties and the facile synthesis method of these types of material.

Nanocrystal perovskite oxide such as lanthanum orthoferrite ($LaFeO_3$) has gained significant attention for its visible light activation and has been utilized in advanced applications such as solid oxide fuel cells [12], gas sensors [13] and photocatalysts [14-17]. The visible light photocatalytic performance of $LaFeO_3$ relies heavily on the structure, morphology and size of the catalyst, which is determined during the synthesis process. The synthesis of $LaFeO_3$ has been reported using numerous methods, with sol-gel considered as a reliable method to produce uniformly sized $LaFeO_3$ nanoparticles due to its simplicity, low equipment requirement, and flexibility to control the synthesis process [18]. Nevertheless, due to its high surface energy, the nanoparticles of $LaFeO_3$ are prone to agglomeration. One method to overcome the agglomeration of nanoparticles is to disperse the nanoparticles onto a support material, which suppresses charge recombination due to the availability of heterojunction for electron and holes. To date, there have been many support materials used to support nanoparticles, for which possessing two-dimensional morphology has shown notable performance increase due to high specific surface area and dispersion capacity.

†To whom correspondence should be addressed.
E-mail: farhana@petroleum.utm.my, farhanaaziz@utm.my

Graphene oxide (GO) has attracted huge attention due to its characteristics for photocatalytic application, including high surface area, high thermal stability, high electron mobility and electron conductivity [19]. GO molecular plane possesses many oxygen functionalities and can be produced in large quantities and dispersed in various solvents [20]. Recent studies have outlined that the GO-supported photocatalyst produced notable photocatalytic performance mainly due to the enhancement in adsorption rate of pollutant and light absorptivity of the composite [21]. Since nanoparticle $LaFeO_3$ has been proven to be effective in the degradation of dye water, GO supported $LaFeO_3$ can be possibly applied with the synergistic advantage of visible light photocatalysis and adsorption.

In this study, we first demonstrated the fabrication of integrated photocatalyst-adsorbents (IPCA) where photocatalyst $LaFeO_3$ is assembled on the surface of GO sheets. Photocatalytic activity of IPCA was performed by the photodegradation of methylene blue under visible light irradiation and compared with nanoparticle $LaFeO_3$. The interface structure of IPCA composite was investigated by using FTIR, XRD, TEM and FESEM. This composite material shows better adsorption capabilities and faster degradation mechanism compared to bare $LaFeO_3$.

EXPERIMENTAL

1. Synthesis of $LaFeO_3$ Powders

The $LaFeO_3$ powders were synthesized by using sol-gel glucose method [22]. Equimolar amounts of Lanthanum nitrate hexahydrate ($La(NO_3)_3{\cdot}6H_20$) and Iron (III) nitrate nonahydrate ($Fe(NO_3)_3{\cdot}9H_2O$) were added into 80% glucose solution at 60 °C. The molar ratio of glucose to metal ions (glucose/M) was 3 : 10. After both salts were completely dissolved in the glucose solution, the temperature was raised to 70 °C to evaporate excess water, and the solution viscosity increased continuously. A gel was formed with the formation of violent NO_x gas resulting from the decomposition of nitrate ions. The samples were then heated in an oven at 250 °C for 2 hours. The resulting specimen was ground into fine powder to obtain the $LaFeO_3$ precursor. Then, the precursor was calcined at 500 °C for two hours to obtain $LaFeO_3$ powders.

2. Formation of Integrated Photocatalyst Adsorbents (IPCA) Composites

The IPCA was formed by using methods as in a previous study [23]. Graphene oxide (GO) was obtained by using modified Hummer's method [24]. To synthesize the IPCA composites, first, GO was suspended in 25 ml deionized water by using a magnetic stirrer. The content of GO was measured at 5% from the total weight of the composite. Calculated amount of $LaFeO_3$ was then dissolved in another 25 ml of deionized water and both solutions were consequently mixed using a sonicator for 2.5 hours. The solution was further mixed with a magnetic stirrer for another 24 hours at room temperature to obtain a homogeneous solution. This was then centrifuged and filtered using ethanol and dried at 65 °C for 8 hours to obtain the IPCA composite.

3. Visible-light Photocatalytic Measurements

The photocatalytic degradation of methylene blue was evaluated to compare the photocatalytic activity between the synthesized $LaFeO_3$ and IPCA composite as photocatalyst. The experiment was contained in a stainless steel box with an access door (Fig. 1). The visible light irradiation, placed 10 cm from the specimen, was sourced from halogen floodlight lamp double ended (Phoenix Electric Co., Ltd. Himeji Japan, λ>420 nm, 300 W, light intensity 96 mW/cm^2). 0.1 g of catalyst was dispersed in 100 ml of methylene blue and the solution was allowed to reach adsorption/desorption equilibrium for 30 min with continuous stirring, prior to the degradation process. After the irradiation source was turned on, a 3 ml sample was withdrawn from the solution by using filtered syringe at 20 min intervals for two hours with continuous stirring, beginning at t_0=0 min (C_0). The photocatalytic degradation efficiency was measured in the decrease of the methylene blue concentration by using Perkin Elmer Lambda 25 UV-Vis spectrometry. The absorbance of methylene blue was observed at 660 nm. The

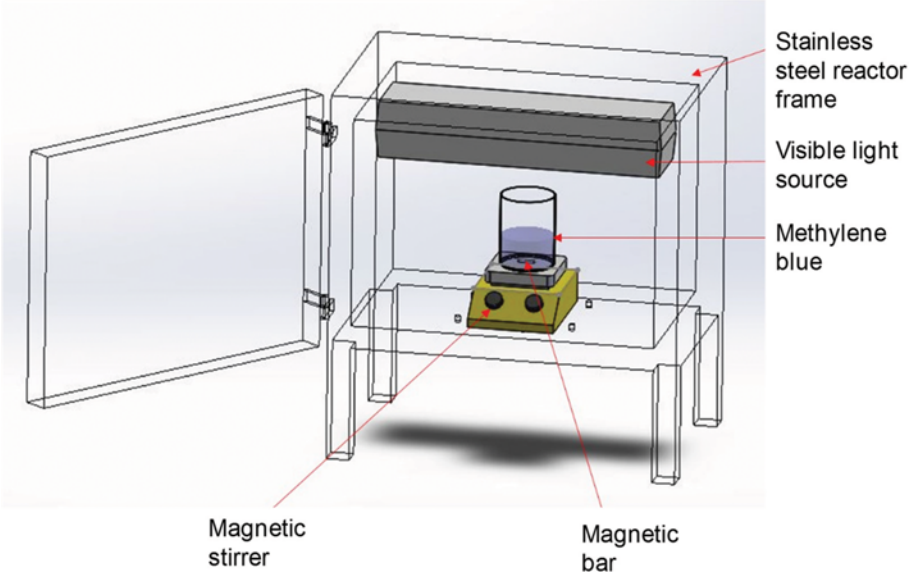

Fig. 1. Photocatalytic reactor with visible light source.

photocatalytic activity was expressed in the percentage of methylene blue degradation according to the following equation (Eq. (1)):

$$\text{Degradation of methylene blue} = \frac{C_0 - C_t}{C_0} \times 100\% \quad (1)$$

where C_0 is the initial concentration at time t=0, and C_t represent the concentration at time interval. Both catalysts ($LaFeO_3$ and IPCA composite) follow the same experimental procedure. A blank experiment was also conducted under no influence from any catalyst to show the methylene blue spontaneous degradation under visible light irradiation.

4. Characterization

The UV-Vis spectrum of the sample was analyzed using Perkin Elmer Lambda 25 UV-vis spectroscopy. Fourier transform infrared spectra (FTIR) of the samples were obtained between 4,000 cm^{-1} and 500 cm^{-1} on a Nicolet Nexus 5700 FTIR spectrophotometer using KBr pellets. X-ray diffraction (XRD) patterns of the samples were analyzed on a Rigaku Smartlab D/MAX 2500 X-ray diffractometer with Cu $K_{\alpha 1}$ radiation (λ=0.1541 nm, scanning step= 1°/min), scanning over the range of $10^{\circ} \leq 2\theta \leq 80^{\circ}$. The morphology of the samples was observed using FESEM (Supra 35-VP, Carl Zeiss, Germany). The Brunauer-Emmett-Teller (BET) specific surface area was determined by using nitrogen gas adsorption method. Transmission electron microscope (TEM) images were obtained on a JEOL ARM- 200F atomic resolution analytical microscope.

RESULTS AND DISCUSSION

1. Optical Properties Analysis

UV-Vis Spectroscopy was used to obtain the optical properties

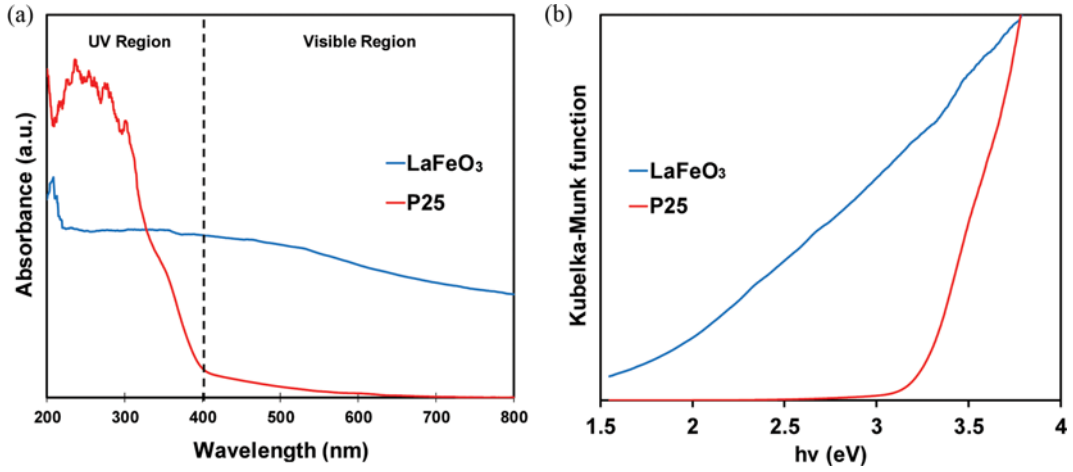

Fig. 2. (a) UV-visible absorption spectra of $LaFeO_3$ and P25 (TiO_2). (b) Kubelka-Munk function of $LaFeO_3$ and P25 to estimate the band gap value.

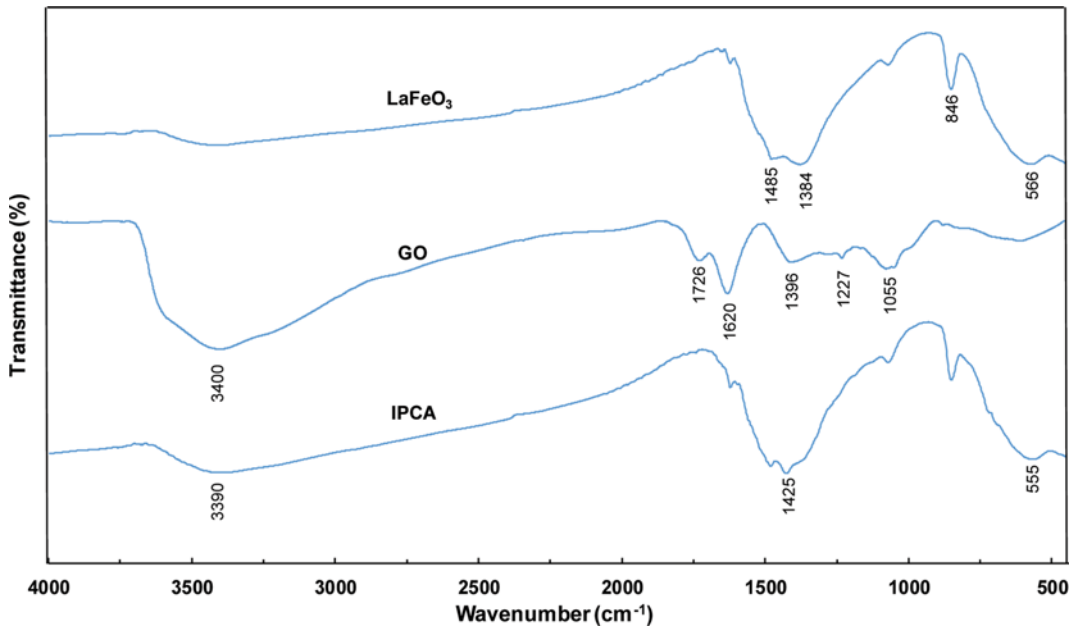

Fig. 3. FTIR spectrum of $LaFeO_3$, GO and IPCA composite.

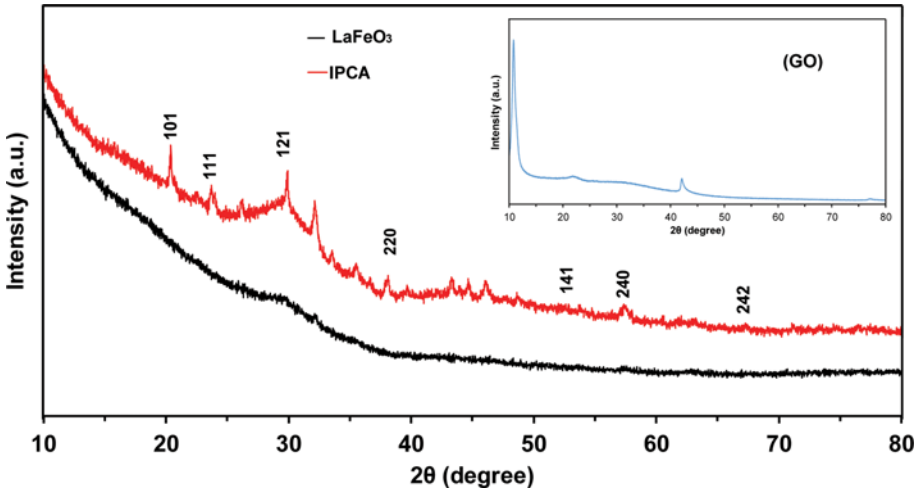

Fig. 4. XRD pattern of $LaFeO_3$ and IPCA composite with GO in the inset.

of the photocatalyst $LaFeO_3$ and compared with a commercial TiO_2 photocatalyst (P25). Fig. 2(a) shows the absorption spectra of both $LaFeO_3$ photocatalyst and P25 over wavelengths at UV and visible light region. As expected, the P25 showed a high adsorption capacity in UV region while performing poorly in the visible light region. Meanwhile, $LaFeO_3$ absorption spectra showed high absorption spectra in both UV and visible light regions. This suggests that the fabricated $LaFeO_3$ photocatalyst would perform photodegradation of pollutants in visible light irradiation as reported elsewhere [25,26]. The Kubelka-Munk function was used to estimate the band gap of the fabricated photocatalyst. According to Fig. 2(b), the estimated value of band gap for $LaFeO_3$ is 2.0 eV, which is relatively lower than P25 at 3.24 eV. The low band gap value of $LaFeO_3$ supported the visible light-driven characteristics of the synthesized photocatalyst.

2. FTIR Spectroscopy

To understand the interface characteristics of the composite IPCA, FTIR analysis was carried out. The FTIR spectra clearly show the vibrational bands of $LaFeO_3$, GO and IPCA (Fig. 3). Basically, the vibrational pattern of the fabricated IPCA indicates higher resemblance towards the $LaFeO_3$ vibrational pattern, which is probably due to the higher amount of $LaFeO_3$ used in the composite (5% GO). For $LaFeO_3$, the characteristic band at 566 cm^{-1} corresponds to the Fe-O stretching vibrations, which is attributed by the octahedral FeO_6 group in the perovskite compounds [6]. The band at 3,390 cm^{-1} is attributed to the O-H in absorbed water and hydroxyl groups. The bands at 1,485 cm^{-1} and 1,384 cm^{-1} are attributed to the splitting of asymmetric stretching of carbonates, which indicates La-carbonate species were formed on the surface of the perovskite due to the exposure to the surrounding atmosphere [25]. The surface of the $LaFeO_3$ is prone to chemisorption of CO_2 gases in ambient, which leads to the formation of carbonate ions [27]. The band at 846 cm^{-1} was due to carbonates [28]. In the vibration band of GO, broad peak at 3,400 cm^{-1} represents the O-H stretching, 1,726 cm^{-1} corresponds to carbonyl stretching, 1,396 cm^{-1} and 1,227 cm^{-1} is attributed to C-OH and C-O-C stretching vibrations, respectively [23]. At 1,055 cm^{-1} shows the vibration band that corresponds to the C-O stretching that denotes the presence of epoxide group in the GO layers and the 1,620 cm^{-1} peak is due to the presence of absorbed water and the skeletal oxidation of unoxidized graphite [29,30]. In the FTIR spectra of the IPCA composite, it was reported that some of the peaks had shifted to lower frequency, such as 3,400 cm^{-1} to 3,390 cm^{-1} (O-H), 1,485 cm^{-1} to 1,425 cm^{-1} (carbonates) and 566 cm^{-1} to 555 cm^{-1} (Fe-O). This is most probably due to strong interaction between the $LaFeO_3$ and GO matrix in the IPCA [31]. The FTIR spectrum indicates that the photocatalyst $LaFeO_3$ has successfully been embedded at the surface of the GO sheets.

3. XRD Spectrum

The XRD spectrum of $LaFeO_3$, GO and IPCA was determined in order to observe the crystallinity of the composite IPCA. Fig. 4 shows the XRD spectrum of $LaFeO_3$ and IPCA composite with GO in the inset. The observed patterns were all indexed with JCPDS card no. 37-1493. The GO spectrum shows a significant diffraction peak at approximately 10.84° at the 2θ, which corresponds to GO [24]. From the figure, due to the calcination temperature of 500 °C, the fabricated $LaFeO_3$ using sol gel glucose method was in amorphous form. The XRD patterns show broad XRD peak with low intensity, which indicates poor crystallinity of the photocatalyst. Although several studies have reported the formation of nanocrystalline $LaFeO_3$ at 500 °C [22,32], most of others [6,25,26,33] only obtained highly crystalline photocatalyst at higher calcination temperature, which is consistent with this study. Nevertheless, the role of photocatalyst crystallinity has been carefully explained by a previous study [34].

Crystallinity is a complex factor affecting the photocatalytic activity. While high crystallinity promotes charge transfer from the center of the surface of catalyst and enhances the photocatalytic activity [35], performance enhancement has also been reported in low crystallinity specimens where the presence of surface defects (impurities, macrovoids, and oxygen vacancies) provides active centers for degradation of pollutants [36]. However, when compared directly between these two, mesoporous catalyst was found to outperform its higher crystallinity counterparts. This phenomenon

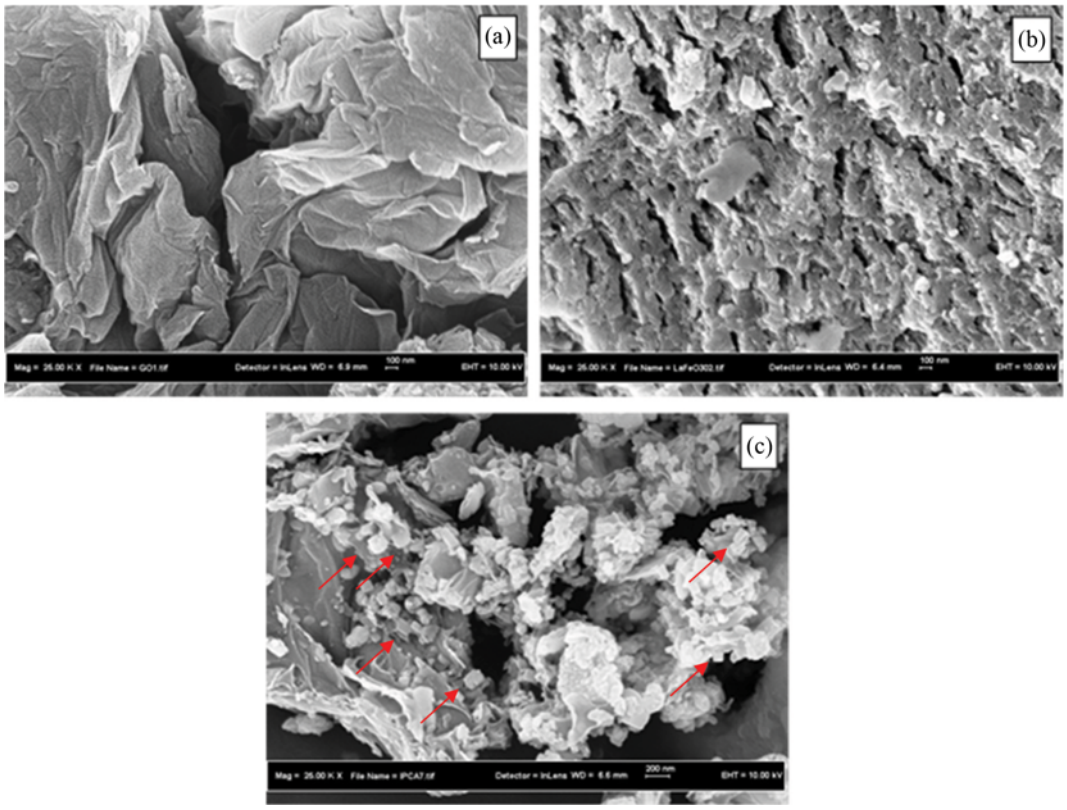

Fig. 5. FESEM images of (a) GO sheets, (b) $LaFeO_3$ powder, and (c) IPCA composite.

was largely due to enhanced light absorption in hierarchical structure, high photocatalytic reaction sites (defects) and large surface area for increased catalytic active sites and assistance in photoinduced charge separation [34]. Additionally, the XRD spectrum of the IPCA composite shows low crystallinity, and diffraction peaks of GO were not detected in the composite spectrum. This is most probably due to low amount of GO added into the composite mixture. However, the crystallinity of IPCA was slightly improved when GO was added to the photocatalyst. This is probably due to photocatalyst $LaFeO_3$ being exposed when assembled on GO sheets. The interaction of GO and $LaFeO_3$ was further identified by using FESEM images.

4. Morphological Study

The morphological changes of the samples were observed by using FESEM. In Fig. 5(a), the features of GO sheets were observed to possess thin wavy sheets (crinkled) with high surface area. The perovskite $LaFeO_3$ prepared by using sol-gel glucose method exhibits particle agglomeration with porous structure (Fig. 5(b)). Based on Fig. 5(c), the perovskite $LaFeO_3$ has been successfully assembled on the surface of GO sheets. It is clear that the agglomeration of $LaFeO_3$ was improved by spreading the catalyst particles onto the high surface area of GO sheets with its nanocube structure

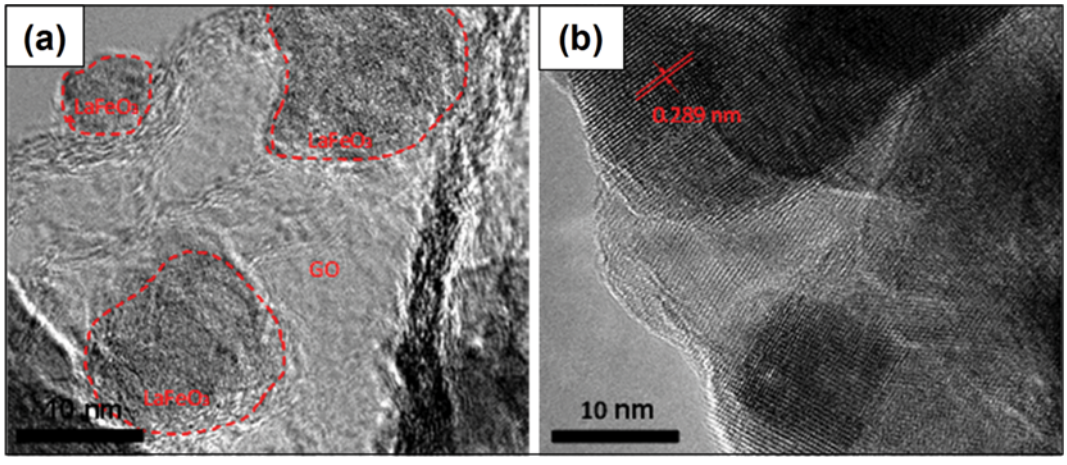

Fig. 6. HR-TEM images of (a) IPCA and (b) $LaFeO_3$ photocatalyst, respectively.

clearly observed (red arrow). Therefore, the fabricated IPCA has proven to potentially possess larger surface area and thus attain more catalytic reaction sites. This observation is also found in other literatures where the incorporation of photocatalyst on high surface area network has produced better photocatalytic activity [6,23].

The solid interiors and more insight of the IPCA were further characterized by high resolution (HR)-TEM technique. Prior to the characterization, the samples were dispersed in EtOH and sonicated for 30 min. From the HR-TEM image in Fig. 6(a), it is revealed that the resultants $LaFeO_3$ was successfully grown on the GO surface. On top of that, well developed interfaces between $LaFeO_3$ and GO also are clearly observed. This observation is consistent with FTIR analysis. Furthermore, the HR-TEM (Fig. 6(b)) shows that the $LaFeO_3$ resembles a cube-shape nanostructured with clear alignment of the lattice fringes confirming the polycrystalline nature [37]. Moreover, the regular spacing of the observed lattice plane was 0.289 nm, which indicated (110) lattice spacing of cubic $LaFeO_3$ [38]. The BET measurement showed that the specific surface area for $LaFeO_3$ is 3.89 m^2/g, while the IPCA recorded a specific surface area value of 18.61 m^2/g. It was stated that the photocatalytic activity is closely related to the surface area and particle size [25]. The difference in specific surface area value is most probably due to the introduction of GO which has improved the specific surface area of the photocatalyst by more than four times of its original value. It is expected that further improvement in specific surface area can be achieved by optimizing the synthesis method of the $LaFeO_3$.

5. Photocatalytic Measurements

The photocatalytic activity of IPCA was evaluated by observing the degradation of methylene blue as a model pollutant, and the

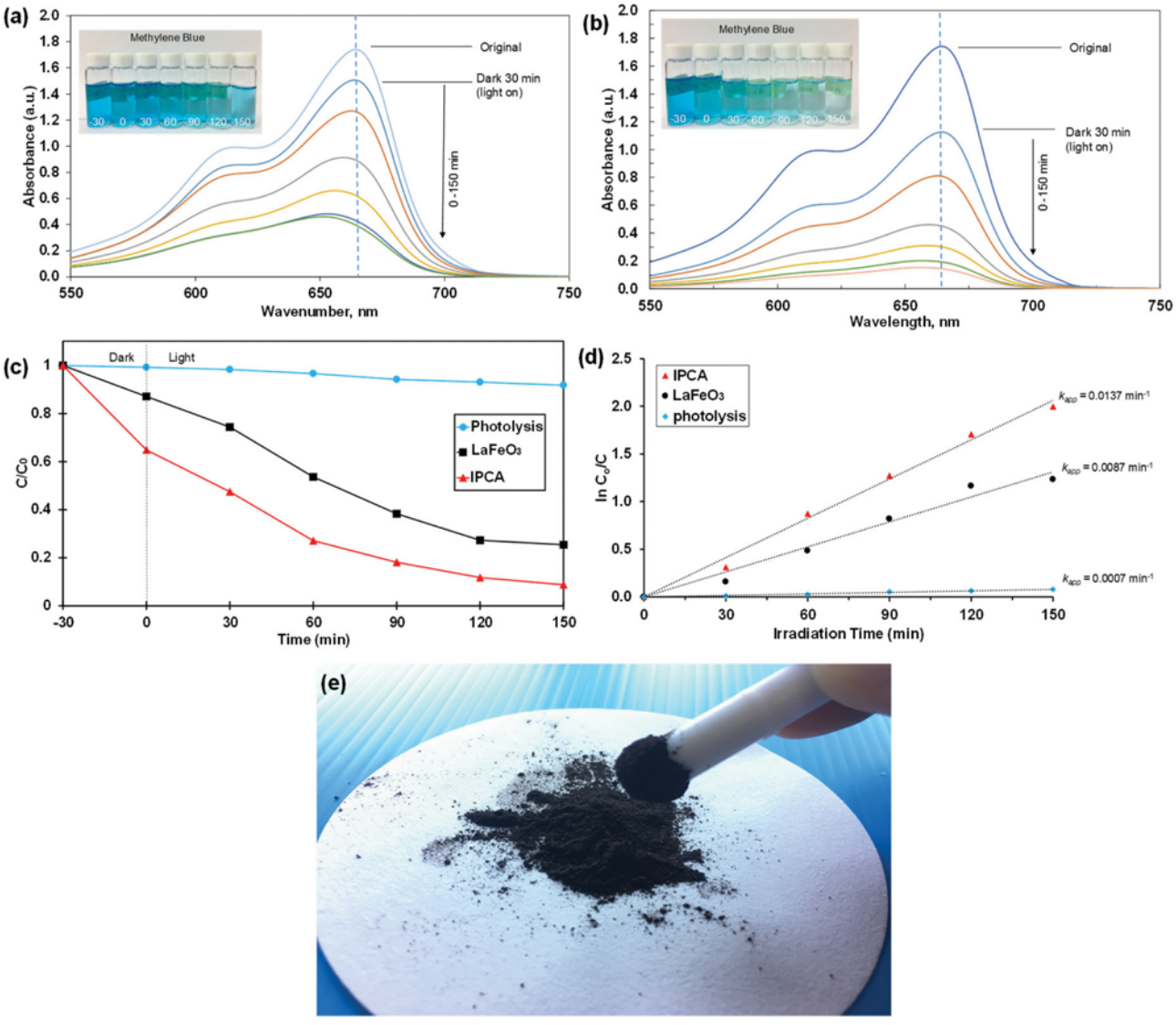

Fig. 7. UV-vis spectrum of methylene blue dye degradation using (a) $LaFeO_3$ and (b) IPCA as photocatalyst under visible light irradiation, (c) photocatalytic degradation of methylene blue values with respect to time measured at 660 cm^{-1}, and (d) kinetic disappearance of methylene blue by IPCA, $LaFeO_3$ and photolysis under visible light irradiation. (e) IPCA can be attracted by magnet in the magnetic stirrer bar.

result was compared with $LaFeO_3$ photocatalyst (Fig. 7). Additionally, photolysis (without photocatalyst) under the same visible light irradiation was also observed to prove that the methylene blue used is relatively stable under visible light irradiation. 30 minutes was allocated for the adsorption of methylene blue, and then photocatalysis proceeded under visible light at t=0. Fig. 7(a) and (b) show the temporal evolution of the UV-Vis adsorption spectra of methylene blue during the photocatalytic reaction of each photocatalyst. Methylene blue solution shows a major adsorption peak at wavelength 660 nm. In addition, a parallel decrease in peak intensities and slight blue shift of the band located at 660 nm can be observed for both samples. This is due to the N-demethylated degradation of methylene blue derivatives, concomitantly with the hypsochromic shifts that occurred gradually [39-41]. In the adsorption phase, the adsorption efficiency of IPCA and $LaFeO_3$ was 35.26% and 12.89%, respectively (Fig. 7(c)). Photocatalyst IPCA was able to produce an overall removal rate of 91.2% in 150 min under visible light irradiation. On the other hand, photocatalyst $LaFeO_3$ was able to attain 74.6% overall removal rate. IPCA showed a greater photocatalytic reaction rate than $LaFeO_3$ most probably due to the presence of graphene oxide. This phenomenon proves the synergistic effect present between $LaFeO_3$ and GO.

The kinetic disappearance of methylene blue with photocatalyst $LaFeO_3$, IPCA and photolysis under visible light irradiation is shown in Fig. 7(d). The photodegradation of methylene blue can be assumed as pseudo-first-order kinetics model, thus assumed as follows: [42]

$$r = \frac{dC_t}{dt} = kC_t \tag{2}$$

$$\ln\left(\frac{C_0}{C_t}\right) = k_{app}t \tag{3}$$

where r is the reaction rate, C_t is the concentration of methylene blue at reaction time t, C_0 is the initial concentration of methylene blue and k_{app} is the apparent time constant. For our measurements, the apparent time constant was 0.0137 min^{-1}, 0.0087 min^{-1} and 0.0007 min^{-1} for IPCA, $LaFeO_3$ and photolysis, respectively. In general, both photocatalysts displayed similar photocatalytic reaction pattern under visible light irradiation. However, the photocatalytic activity with IPCA was higher when compared with bare $LaFeO_3$ photocatalyst. These are probably due to the synergistic effect between $LaFeO_3$ and GO present in the IPCA.

Higher efficiency of IPCA was due to the structure of graphene oxide. Graphene oxide has various oxygen functionalities on its planes and sheet surfaces, increases adsorption capability by its high surface area and facilitates the degradation of methylene blue by reducing charge recombination rate [23]. The synergistic effect of IPCA is due to the abundance of hydroxyl groups that trap light holes and generate active hydroxyl radicals [43]. The graphene oxide sheets also prevent agglomeration of $LaFeO_3$ particles, which has been known to cause severe photocatalytic performance degradation of nanoparticle $LaFeO_3$ and distribute the photocatalyst effectively.

The synthesized IPCA has demonstrated increased photodegradation ability in visible light with high adsorption performance of methylene blue compared to the bare photocatalyst. Due to the Fe content in the photocatalyst, the synthesized IPCA was observed to have magnetic properties [44] (Fig. 7(e)). Furthermore, the feasibility of magnetic properties in the IPCA could be an advantage for the application in the wastewater treatment purposes. The IPCA can be dispersed in wastewater system for degradation of pollutants and can be separated effectively using magnets, as compared to conventional photocatalyst, after usage in suspension system. In addition, the IPCA can be redeployed in an aqueous solution after detaching from the magnet using ultrasonic vibration.

The photocatalytic degradation reaction mechanism is schematically illustrated in Fig. 8. The degradation mechanism would possibly occur as follows: (1) Upon irradiation of IPCA by visible light, visible light absorption occurred and excited the electron from valence band (VB) to conduction band (CB), vacating a positive hole in the valance band. (2) The GO promoted the separation of the electrons by migration of electron within GO structure and leaving positive holes at VB to keep them highly reactive, thus preventing the recombination phenomenon of the electron-hole pair. (3) The strong oxidation power of photoinduced holes liber-

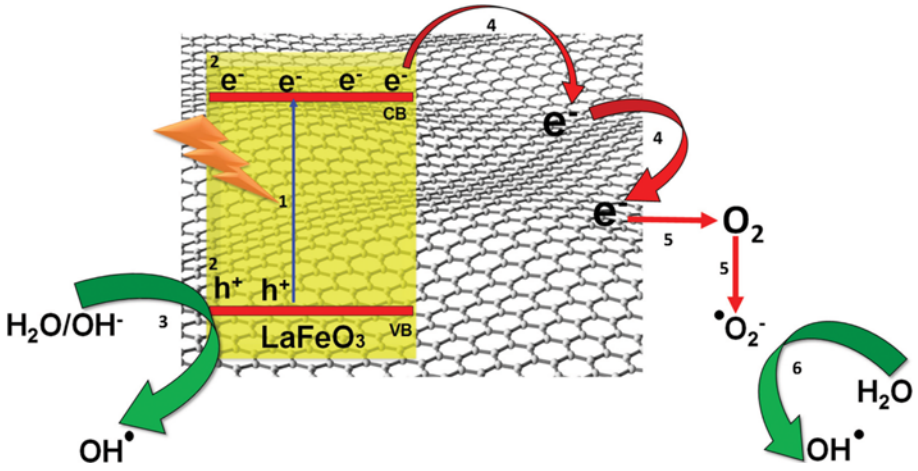

Fig. 8. Illustration of photocatalytic degradation of pollutant by IPCA.

ates an electron from hydroxide ion in water to form OH radicals. (4) The electron continues to migrate until it reacts with the dissolved oxygen. (5) The reaction between migrating electron and dissolved oxygen will produce superoxide radical anions. (6) The superoxide radical anions would possibly lead to the formation of hydroxyl radical [37]. Decomposition of methylene blue occurs when the OH radical procures an electron from a nearby methylene blue to become a stable species. The loss of electron of methylene blue results in mineralization, forming carbon dioxide and water. The high adsorption characteristics of the IPCA photocatalyst would possibly cause a higher concentration of methylene blue at the vicinity of the catalyst, which would enhance the photocatalytic degradation activity.

CONCLUSIONS

Novel integrated photocatalyst-adsorbents (IPCA) composite was successfully prepared by combining the synergistic effects of sol-gel glucose fabricated $LaFeO_3$ and GO. The visible light photocatalytic activity of IPCA is superior to that of bare $LaFeO_3$. The high surface area of GO was successfully assembled with photocatalyst $LaFeO_3$, which enhanced methylene blue adsorption and increased photocatalytic reaction kinetics. We presume that the presence of GO in the composite was responsible for the high reaction activity due to high surface area assembly of perovskite $LaFeO_3$ on GO matrix. With IPCA as the catalyst, we achieved methylene blue removal rate of 91.2% in 150 minutes under visible light irradiation. The presence of hydroxyl groups at high surface area could trap light holes and generate hydroxyl radicals, contributing to the synergistic effect of IPCA to degrade methylene blue. Additionally, the magnetic properties present in the IPCA would allow the photocatalyst to be easily collected after being dispersed in the wastewater suspension. This study points out the potential of combining the synergistic effects between $LaFeO_3$ and GO to develop a high performance photocatalyst, IPCA, for the photodegradation of methylene blue.

ACKNOWLEDGEMENTS

The authors acknowledge the financial support by the Ministry of Higher Education (MOHE) Malaysia under Grant No. R.J090301.7846.4J189 and R.J090301.7846.4J190 and Universiti Teknologi Malaysia (UTM).

REFERENCES

1. L. K. G. Ackerman, M. M. Lovell and D. J. Weix, *Nature*, **524**, 454 (2015).
2. F. Su, X. Lv and M. Miao, *Small*, **11**, 854 (2015).
3. J.-W. Yoon, M.-H. Baek, J.-S. Hong, C.-Y. Lee and J.-K. Suh, *Korean J. Chem. Eng.*, **29**, 1722 (2012).
4. F. Aziz and A. F. Ismail, *Polym. Bull.*, **72**, 1827 (2015).
5. H. Yang and P. Fu, *Surf. Rev. Lett.*, **15**, 337 (2008).
6. K. Peng, L. Fu, H. Yang and J. Ouyang, *Sci. Rep.*, **6**, 19723 (2016).
7. L. Yang, Y. An, B. Dai, X. Guo, Z. Liu and B. Peng, *Korean J. Chem. Eng.*, **34**, 476 (2017).
8. J. M. Abdul, S. Vigneswaran, H. K. Shon, A. Nathaporn and J. Kandasamy, *Korean J. Chem. Eng.*, **26**, 724 (2009).
9. S. Chakma, S. Praneeth and V. S. Moholkar, *Ultrason. Sonochem.*, **38**, 652 (2017).
10. S. Chakma and V. S. Moholkar, *J. Taiwan Inst. Chem. Eng.*, **60**, 469 (2016).
11. S. Chakma and V. S. Moholkar, *J. Ind. Eng. Chem.*, **33**, 276 (2016).
12. L. Liu, K. Sun, X. Li, M. Zhang, Y. Liu, N. Zhang and X. Zhou, *Int. J. Hydrogen Energy*, **37**, 12574 (2012).
13. P. Song, Q. Wang, Z. Zhang and Z. Yang, *Sensors Actuators, B Chem.*, **147**, 248 (2010).
14. P. Tang, Y. Tong, H. Chen, F. Cao and G. Pan, *Curr. Appl. Phys.*, **13**, 340 (2013).
15. Q. Zhang, Y. Huang, S. Peng, Y. Zhang, Z. Shen, J. Cao, W. Ho, S. C. Lee and D. Y. H. Pui, *Appl. Catal. B Environ.*, **204**, 346 (2017).
16. J. Zhu, H. Li, L. Zhong, P. Xiao, X. Xu, X. Yang, Z. Zhao and J. Li, *ACS Catal.*, **4**, 2917 (2014).
17. J. Zhu, Y. Zhao, D. Tang, Z. Zhao and S. A. C. Carabineiro, *J. Catal.*, **340**, 41 (2016).
18. M. A. Mohamed, W. N. W. Salleh, J. Jaafar, A. F. Ismail and N. A. M. Nor, *Mater. Chem. Phys.*, **162**, 113 (2015).
19. Y. Yang, F. Lu, Z. Zhou, W. Song, Q. Chen and X. Ji, *Electrochim. Acta*, **113**, 9 (2013).
20. D. C. Marcano, D. V. Kosynkin, J. M. Berlin, A. Sinitskii, Z. Sun, A. Slesarev, L. B. Alemany, W. Lu and J. M. Tour, *ACS Nano*, **4**, 4806 (2010).
21. Y.-E. Moon, G. Jung, J. Yun and H.-I. Kim, *Mater. Sci. Eng. B.*, **178**, 1097 (2013).
22. T. Liu and Y. Xu, *Mater. Chem. Phys.*, **129**, 1047 (2011).
23. S. Vadivel, M. Vanitha, A. Muthukrishnaraj and N. Balasubramanian, *J. Water Process Eng.*, **1**, 17 (2014).
24. G. S. Lai, W. J. Lau, P. S. Goh, A. F. Ismail, N. Yusof and Y. H. Tan, *Desalination*, **387**, 14 (2016).
25. S. Thirumalairajan, K. Girija, I. Ganesh, D. Mangalaraj, C. Viswanathan, A. Balamurugan and N. Ponpandian, *Chem. Eng. J.*, **209**, 420 (2012).
26. R. Hu, C. Li, X. Wang, Y. Sun, H. Jia, H. Su and Y. Zhang, *Catal. Commun.*, **29**, 35 (2012).
27. S. Farhadi, Z. Momeni and M. Taherimehr, *J. Alloys Compd.*, **471**, 5 (2009).
28. Y.-G. Cho, K.-H. Choi, Y.-R. Kim, J.-S. Jung and S.-H. Lee, *Bull. Korean Chem. Soc.*, **30**, 1368 (2009).
29. M. Hilder, O. Winther-Jensen, B. Winther-Jensen and D. R. MacFarlane, *Phys. Chem. Chem. Phys.*, **14**, 14034 (2012).
30. T. Yang, L. Liu, J. Liu, M.-L. Chen and J.-H. Wang, *J. Mater. Chem.*, **22**, 21909 (2012).
31. M. Zhu, P. Chen and M. Liu, *ACS Nano*, **5**, 4529 (2011).
32. J. Feng, T. Liu, Y. Xu, J. Zhao and Y. He, *Ceram. Int.*, **37**, 1203 (2011).
33. Z. Kaiwen, W. Xuehang, W. Wenwei, X. Jun, T. Siqi and L. Sen, *Adv. Powder Technol.*, **24**, 359 (2013).
34. W. Cen, T. Xiong, C. Tang, S. Yuan and F. Dong, *Ind. Eng. Chem. Res.*, **53**, 15002 (2014).
35. J. B. Joo, Q. Zhang, M. Dahl, I. Lee, J. Goebl, F. Zaera and Y. Yin, *Energy Environ. Sci.*, **5**, 6321 (2012).
36. J. Ma, H. Wu, Y. Liu and H. He, *J. Phys. Chem. C.*, **118**, 7434

(2014).
37. M. A. Mohamed, W. N. Wan Salleh, J. Jaafar, M. S. Rosmi, Z. A. Mohd. Hir, M. Abd Mutalib, A. F. Ismail and M. Tanemura, *Appl. Surf. Sci.*, **393**, 46 (2017).
38. S. Thirumalairajan, K. Girija, N. Y. Hebalkar, D. Mangalaraj, C. Viswanathan and N. Ponpandian, *RSC Adv.*, **3**, 7549 (2013).
39. R. Zuo, G. Du, W. Zhang, L. Liu, Y. Liu, L. Mei and Z. Li, Photocatalytic Degradation of Methylene Blue Using TiO_2 Impregnated Diatomite, **2014**, 1 (2014).
40. C. Wang and J. Yao, *Int. J. Photoenergy*, **2010**, 1 (2010).
41. F. Wang, S. Min, Y. Han and L. Feng, *Superlattices Microstruct.*, **48**, 170 (2010).
42. M. A. Mohamed, W. N. W. Salleh, J. Jaafar, A. F. Ismail, M. A. Mutalib, N. A. A. Sani, S. E. A. M. Asri and C. S. Ong, *Chem. Eng. J.*, **284**, 202 (2016).
43. X. Li and H. Yang, *Appl. Clay Sci.*, **100**, 43 (2014).
44. E. Grabowska, *Appl. Catal. B Environ.*, **186**, 97 (2016).